Microsystem Technologies (2021) 27:251–261
https://doi.org/10.1007/s00542-020-04944-0

TECHNICAL PAPER

Design and optimization of MEMS piezoelectric energy harvester for low frequency applications

A. Nisanth[1] · K. J. Suja[1] · V. Seena[2]

Received: 6 March 2020 / Accepted: 22 June 2020 / Published online: 14 July 2020

Abstract
Piezoelectric vibrational energy harvester (PVEH) suits best for harvesting vibrational energy from the environment due to the simplicity in design, operation, and compatibility with the micro electro mechanical system (MEMS) technology. In this work, the effect of geometrical parameters on the performance of an Aluminium Nitride (AlN) based MEMS PVEH is analyzed in detail and optimized for lower resonant frequency and higher output power. Electromechanical modeling and validation are carried out for an energy harvester with various proof mass shapes. The optimized PVEH is having a trapezoidal beam and a triangular-shaped proof mass. The effect of the amount of proof mass coverage on the performance parameters is also analyzed. The least resonant frequency is found for the design in which the proof mass coverage is 57 % of the overall length of the harvester and the power peaks when the proof mass coverage becomes 80 %. The proposed structure generated output power of 0.24 μW at a resonant frequency of 158.8 Hz when an input acceleration of 0.5 g is applied. Then an array using the proposed structure is simulated and compared to an array of conventional rectangular energy harvesters and it is found that array using the proposed structure provides 1.79 times higher power at a lower resonant frequency than the conventional array.

1 Introduction

Wireless sensor networks (WSN) play a significant role in various application areas such as agriculture, industry, medicine, military, etc (Gilbert and Balouchi 2008). A WSN contains spatially distributed sensors that are used to monitor different parameters and the collected information is passed to the controlling unit with the help of a network. Usually, WSN consists of a large number of nodes that are connected to different types of sensors. A sensor node usually contains a microcontroller, a radio transceiver, an electronic circuit, and a power source. Due to the rapid development in microelectronics technology and low power Very Large Scale Integration (VLSI) technology, the power requirements of these sensors have reduced considerably. The major problem associated with wireless sensor networks is the power supply. These devices are usually powered by standard batteries. When a sensor is depleted of energy, it can't fulfill its role in the WSN unless the source of energy is replenished (Seah et al. 2009). Short lifetime is a major concern as far as the conventional batteries are considered (Roundy et al. 2003; Roundy and Wright 2004). Therefore, the periodical replacement of these batteries is a must for the proper functioning of the sensors. But the replacement process is not easy as these sensors are usually deployed in remote locations and harsh environments. Moreover, any defects/breakage in the packaging can result in environmental problems. The lifetime of a wireless sensor network can be increased if the device can be made independent of limited power sources such as batteries. This is the major motivation behind the search for an alternative power source for WSNs. A sensor node can be made autonomous by utilising ambient energy harvesting. The major sources of ambient energy are solar, wind, radiofrequency, temperature difference, mechanical vibration, and movement of human body parts (Priya and Inman 2009). Usually, these

✉ A. Nisanth
sagar.nisanth@gmail.com

K. J. Suja
suja@nitc.ac.in

V. Seena
seena.v@iist.ac.in

[1] Department of Electronics and Communication, National Institute of Technology Calicut, Kozhikode, Kerala, India

[2] Department of Avionics, Indian Institute of Space Science and Technology, Thiruvananthapuram, Kerala, India

devices are used for both indoor and outdoor applications. Therefore, mechanical vibrations are preferred over the others in case of micro energy harvesting (Anton and Sodano 2007; Saadon and Sidek 2011). There are mainly three types of vibrational energy harvesters. They are electromagnetic vibrational energy harvester, electrostatic vibrational energy harvester, and piezoelectric vibrational energy harvester (Wei and Jing 2017). The major advantages of PVEH are high electromechanical coupling, higher power density, ease of integration and does not require any external power source. Recently mechanical energy harvesting using triboelectric nanogenerators (TENG) is also reported (Bai et al. 2013; Sukumaran et al. 2020; Chandrasekhar et al. 2020, 2019, 2017, 2017).

Different structures for energy harvesters have been reported. Most of the research works are based on the cantilever structure with Lead Zirconate Titanate (PZT) as the piezo element (Shen et al. 2009; Yu et al. 2014). Due to the simple structure and the ability to produce a relatively high average strain for a given vibration input, the cantilever beam piezoelectric energy harvester is widely studied and designed. The typical structure of a cantilever-based piezoelectric energy harvester is shown in Fig. 1. It consists of a cantilever structure, which is composed of a structural beam, a piezoelectric layer, and electrodes. One end of the cantilever is fixed (anchor) and the other end is free to move. Usually, the cantilever structure will resonate only at a particular frequency. The piezoelectric layer with top and bottom electrodes is attached to the supporting beam. The proof mass at the free end helps in adjusting the resonant frequency.

When an input acceleration is applied to the structure, the mass converts the input acceleration into force. It will cause the bending of the beam and which in turn will result in a strain distributed along the beam. The displacement of the beam causes the piezo layer to be compressed or tensed. This will create charge accumulation due to the piezoelectric effect. The electrodes are used to tap these charges.

Typical piezoelectric materials that are used for energy harvesting are PZT, Zinc Oxide (ZnO), AlN, Barium Titanate (BaTiO3), and Poly vinylidene Fluoride (PVDF) (Todaro et al. 2017; Toprak and Tigli 1989). Thin films and multi-layered hetero structures of piezoelectric materials are used for MEMS applications. It is because they can be micromachined without decreasing their electromechanical coupling (Eom and Trolier-McKinstry 2012). PZT is the widely used piezoelectric material than the other materials due to its high electromechanical coupling coefficient. But the main issue with PZT is the presence of Lead (Pb), which is highly toxic and causes environmental pollution. Thus the design of a piezoelectric energy harvester by utilising lead-free materials to obtain low frequency and high output power is a real challenge.

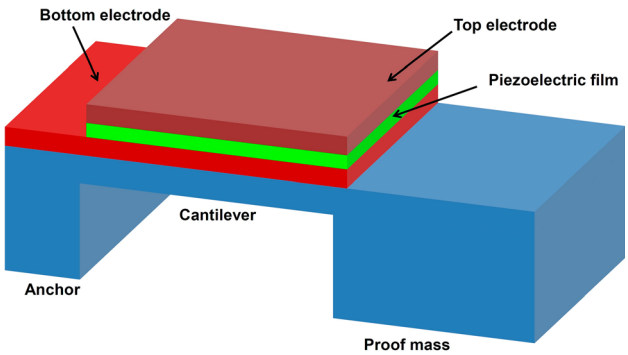

Fig. 1 Structure of a piezoelectric vibration energy harvester

There are mainly two modes of operation for a piezoelectric energy harvester depending upon the stress and polarisation direction. They are d_{31}, and d_{33} modes (Kim et al. 2012). For poling PVEH to d_{33} piezoelectric mode high voltages are required but at such high voltage device may fail because of electric breakdown. In terms of power and voltage d_{33} mode provides better performance than d_{31} mode, but d_{31} mode provides better current. But despite its low performance in power and voltage when compared with d_{33} mode, d_{31} mode is widely used in PVEH because of its simplicity in fabrication (Ramsay et al. 2001).

Most of the MEMS scale piezoelectric energy harvesters reported so far is having low output power and high resonant frequency. Research works are now focused on designing miniaturised energy harvesters with higher power density at low frequencies. The generated output power of the harvester depends upon the device geometry, stress distribution, and effective mass. In literature, different beam geometries have been studied in detail and the shape of the proof mass used is rectangular or square (Jia and Seshia 2016; Zhang et al. 2017; Jackson et al. 2014; Sordo et al. 2016). There are only a few studies that investigate the effect of other shapes of the proof mass on the performance of the piezoelectric energy harvesters (Saxena and Sharma 2014; Alameh et al. 2018; Nisanth et al. 2018). In this work, the effect of the shape of the proof mass on the resonant frequency and output power are studied. An energy harvester using a trapezoidal beam and triangular proof mass is proposed for the first time, which has the advantage of lower resonant frequency and better suitability for array design than the conventional harvester with a rectangular beam and rectangular proof mass. In this work, Aluminium Nitride (AlN) is used as the piezoelectric element as aluminium nitride shows better stability at elevated temperatures. The melting point of AlN is 2100 ^{o}C. Also AlN exhibits piezoelectric properties at temperatures up to 1150 ^{o}C (Fei et al. 2018).

This paper is structured in the following way: initially the working principle of a piezoelectric energy harvester with a proof mass is explained then the simulation results for beam geometry analysis, proof mass geometry analysis,

optimization of energy harvester, array design is presented, followed by the electromechanical modeling and validation of the effect of proof mass shape on the performance parameters and conclusion.

2 Design of the PVEH

The important parameters considered in this work for designing PVEH are output power and resonant frequency. Optimization aims to achieve lower resonant frequency and higher output power. The resonant frequency of the device mostly depends on the device geometry. The length, width, and thickness of the beam have a predominant effect on the resonant frequency. Ideally for the device to have the least possible resonant frequency the device should be long, narrow and thin (Yu et al. 2014). But practical stability of the device also has to be considered.

Another design parameter is the output power, this depends on the overall stress distribution on the beam or the piezoelectric layer. As output power is directly proportional to the amount of stress exerted, the geometry that allows maximum stress within the fracture limit gives the maximum output power. Two parameters of the device geometry are considered for optimization, the shape of the beam and shape of the proof mass.

2.1 Resonant frequency

The resonant frequency is an important performance parameter of a PVEH. The device will provide maximum output power at the resonant frequency and as the excitation frequency moves away from the resonant frequency output power will decrease. The equation for equivalent stiffness for a cantilever beam, when subjected to vertical harmonic excitation is given in Eq. (1) (Yu et al. 2014):

$$k_{eq} = \frac{3EI}{L^3} \tag{1}$$

where I is the equivalent moment of inertia, E is the equivalent Young's modulus, and L is the equivalent beam length. The value of EI for a composite beam can be calculated by Eq. (2)

$$\begin{aligned} EI =& E_p W_p h_p \left[(z_{pN} - z_N)^2 + \frac{(h_p)^2}{12} \right] \\ &+ E_s W_s h_s \left[(z_{sN} - z_N)^2 + \frac{(h_s)^2}{12} \right] \end{aligned} \tag{2}$$

where h_s and h_p are the thickness of the silicon substrate and piezoelectric layer respectively. z_{pN} and z_{sN} are the neutral axis of the piezoelectric layer and silicon substrate respectively. E_s and E_p are Young's modulus of the silicon beam and the piezo material respectively. z_N is the neutral axis of the total piezoelectric cantilever.

The general expression for resonant frequency is given by Eq. (3) (Yu et al. 2014).

$$w_n = \sqrt{\frac{k_{eq}}{m}} \tag{3}$$

where k_{eq} is the equivalent stiffness of the structure and m is the mass. Therefore the resonant frequency of the piezoelectric cantilever is given by Eq. (4) (Yu et al. 2014).

$$w_n = \sqrt{\frac{3EI}{(m_{pm} + \frac{33}{140} m_b) L^3}} \tag{4}$$

where m_{pm} and m_b are the mass of the proof mass and piezoelectric beam respectively.

2.2 Output power

The power obtained from an energy harvester can be expressed through Eq. (5) (Roundy et al. 2003; Williams and Yates 1996; Beeby et al. 2006).

$$P = \frac{m_e \zeta_e Y^2 (\frac{\omega}{\omega_r})^3 \omega^3}{\left[1 - \left(\frac{\omega}{\omega_r}\right)^2\right]^2 + \left[2\zeta_T \frac{\omega}{\omega_r}\right]^2} \tag{5}$$

Where ζ_T is the total damping ratio;($\zeta_T = \zeta_e + \zeta_p$), ζ_e and ζ_p are the electrical and the mechanical damping ratio respectively; m_e is the equivalent mass; ω and Y are excitation frequency and the amplitude of vibration respectively. Output power reaches its peak when the external vibration frequency becomes equal to the resonant frequency ($\omega = \omega_r$) of the device. Maximum output power can be expressed as in Eq. (6) (Roundy et al. 2003; Williams and Yates 1996; Beeby et al. 2006).

$$P_{max} = \frac{m_e \zeta_e Y^2 \omega_r^3}{4\zeta_T^2} \tag{6}$$

For a given mechanical damping, the maximum output power occurs when the electrical damping becomes equal to the mechanical damping. ie ($\zeta_e = \zeta_p = \zeta$). Maximum output power can be expressed in terms of load acceleration magnitude, it is given in Eq. (7) (Roundy et al. 2003; Williams and Yates 1996; Beeby et al. 2006).

$$P_{max} = \frac{m_e A^2}{16\zeta\omega_r} \tag{7}$$

Where A is load acceleration magnitude and it is given as $A = \omega_r^2 Y$. Thus, from Eqs. (4) and (6), it is evident that the performance parameters of the harvester depend upon the device's geometrical parameters.

From Eq. (4) it can be observed that the resonant frequency will decrease as the device length and mass increase. From Eqs. (6) and (7) it is evident that output power is directly proportional to the mass (m_e). Thus the proof mass geometry will affect the resonant frequency of the energy harvester. Therefore the modeling of the effect of proof mass geometry on resonant frequency is of much importance. Tuning of resonant frequency by adjusting the proof mass shape will provide more flexibility in designing a PVEH.

3 Finite element analysis and results

Modeling of the energy harvester and analysis of performance parameters such as resonant frequency and output power are carried out using the finite element tool CoventorWare®10.2. Here a multi-layered cantilever structure is designed. This multi-layered structure consists of SiO_2/Si/SiO_2/Ti/Pt/AlN/Pt in the same order from bottom to top. The cross-sectional view of PVEH is given in Fig. 2.

The details of various layers used and their corresponding thickness used in the simulation are given in Table 1.

For all the simulations of the MEMS PVEH, load acceleration of 0.5 g (g = 9.8 m/s^2) and a damping ratio of ζ=0.01 is used.

3.1 Beam geometry analysis

In order to identify the effect of beam geometry on performance parameters three types of beam shapes namely Rectangular, Trapezoidal and Reverse trapezoidal are selected. The beam length, the anchor side width, and mass are kept constant in this analysis. Fig. 3 shows the structure of different beam geometries.

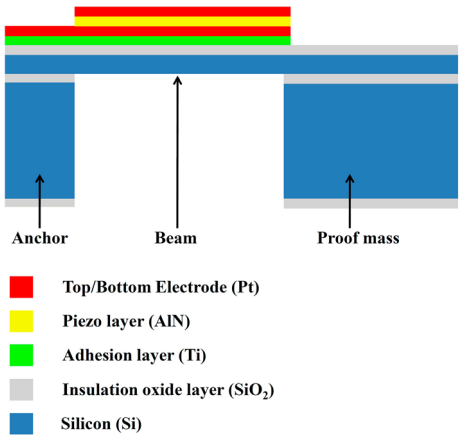

Fig. 2 Cross-sectional view of PVEH

Table 1 Layer details of the energy harvester

Parameter	Value
Thickness of silicon substrate	500 μm
Thickness of oxide layer	0.5 μm
Thickness of silicon beam	20 μm
Thickness of adhesion layer	10 nm
Thickness of AlN	1.0 μm
Thickness of top/bottom electrode	120 nm

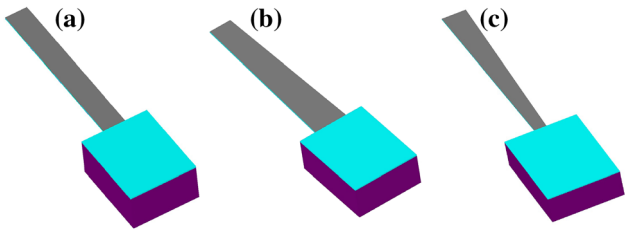

Fig. 3 Different shapes of beam: (**a**) Rectangular, (**b**) Reverse trapezoidal, (**c**) Trapezoidal

Table 2 Material properties

Parameter	Value
Density of Silicon (kg/m^3)	2330
Density of AlN (kg/m^3)	3200
Young's Modulus of AlN (GPa)	345
Young's Modulus of silicon (GPa)	170

Dimensions of the three types of beams are given in Table 3. The length of the beam is kept at 3200 μm. The length and width of the proof mass are kept at 1600 μm and 1200 μm respectively for all the three beam geometries. From Table 3, it can be observed that the energy harvester with a trapezoidal-shaped beam provides a lower resonant frequency than the other types. This decrease in frequency is due to the reduction in the stiffness of the beam.

Harmonic analysis is conducted to determine the influence of beam geometry on output power. Figure 4 displays the comparison of the stress profile for the three beam geometries. From Fig. 4 it can be observed that the stress profile is more uniform in the case of a trapezoidal beam

Table 3 Device dimensions for the three types of beams and corresponding resonant frequencies

Beam shape	Fixed end Width (μm)	Free end width (μm)	Resonant frequency (Hz)
Rectangular	400	400	176.4
Trapezoidal	400	200	160.4
Reverse trapezoidal	400	600	189

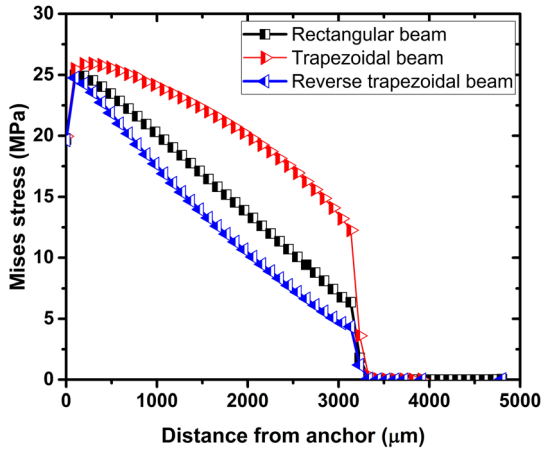

Fig. 4 Stress profile comparison for the three energy harvesters

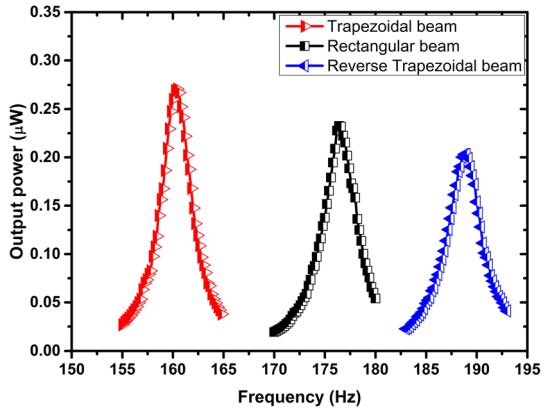

Fig. 5 Power Vs Frequency plots for beam geometry analysis

than the other types, which will result in increased output power.

The graph of Power Vs Frequency for beam geometry analysis is shown in Fig. 5.

From the above analysis, it is observed that the trapezoidal-shaped beam provides better output power at a lower resonant frequency. The maximum output power obtained is 0.27 μW, 0.23 μW and 0.20 μW for the trapezoidal, rectangular and reverse trapezoidal beams respectively.

3.2 Proof mass geometry analysis

In this analysis, three different shapes of proof mass are considered they are rectangular, triangular and semi-circular. The total volume of the proof mass is kept the same for all three cases. The dimensions of the three proof mass geometries and the corresponding resonant frequencies are given in Table 4 and the simulated structures of the three types of proof mass geometries are shown in Fig. 6.

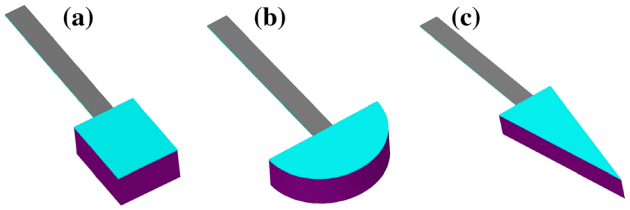

Fig. 6 Different shapes of proof mass: (**a**) Rectangular, (**b**) Semi-circular, (**c**) Triangular

For all three shapes of the proof mass, the rectangular-shaped beam was used. The length and width of the beam are kept at 3200 μm and 400 μm respectively, for all the three proof mass geometries.

From the analysis performed it is possible to observe that the energy harvester with a triangular proof mass achieves the least resonant frequency. Therefore, a triangular proof mass instead of traditional rectangular proof mass can be used to achieve the lowest resonant frequency for a given mass. This decrease in resonant frequency is due to an increase in the harvester's overall length for a triangular proof mass.

The Power Vs Frequency plots for proof mass geometry analysis of rectangular, semi-circular and triangular-shaped proof masses are shown in Fig. 7.

The maximum output power obtained is 0.25 μW, 0.23 μW and 0.20 μW for the triangular, rectangular and semi-circular proof masses respectively. From the above study, it can be inferred that triangular-shaped proof mass gives better output power at a lower resonant frequency than the rectangular and semi-circular proof mass.

3.3 Energy harvester optimization

It can be inferred from the above two analyses that a combination of a trapezoidal cantilever and a triangular proof mass will be a better option for attaining a lower resonant frequency. Thus an energy harvester which consists of a trapezoidal beam and a triangular proof mass (structure-1) is designed and simulated. The simulated structure is shown in Fig. 8.

Table 4 Dimensions of the different proof mass geometries and corresponding resonant frequencies

Proof mass shape	Length (μm)	Width (μm)	Resonant frequency (Hz)
Rectangular	1600	1200	176.4
Semi-circular	1105.58	2211.16	201.4
Triangular	3200	1200	158.2

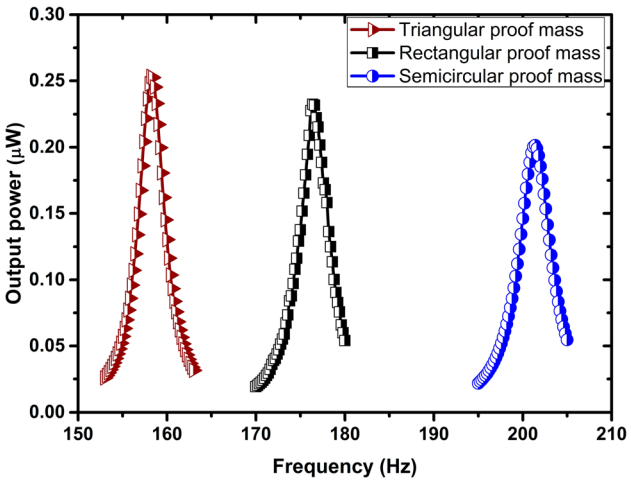

Fig. 7 Power Vs Frequency plots for proof mass analysis

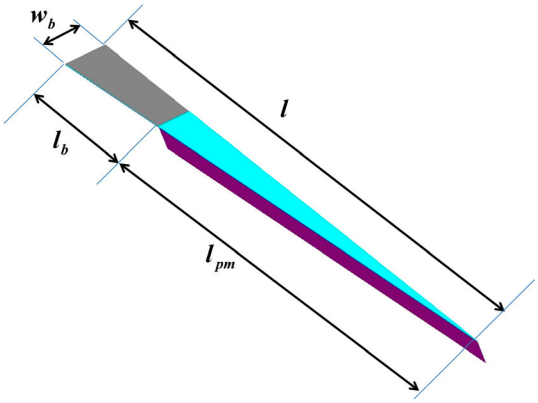

Fig. 8 Simulated structure of energy harvester with trapezoidal beam and triangular proof mass-(structure-1)

The device dimensions are selected such that structure -1 is having the same area/volume as that of the basic rectangular beam with rectangular proof mass discussed in 3.1 and 3.2. For the rectangular beam with the rectangular proof mass structure, the width of the proof mass is more than the beam width. Thus there is a discontinuity at the beam-proof mass interface. Whereas in the proposed structure there is no discontinuity at the beam -proof mass interface. The proof mass is an exact continuation of the beam. The proposed energy harvester is 10 mm in length *(l)* and the width at the fixed end (w_b) is 640 μm. The beam length (l_b) is 2250 μm.

The plot between output power and frequency for structure-1 at the optimum load resistance condition is shown in Fig. 9. The proposed structure was able to generate an output power of 0.24 μW at a resonant frequency of 158.8 Hz. From this analysis, it can be observed that the proposed structure was able to generate higher power at a lower resonant frequency than the conventional energy

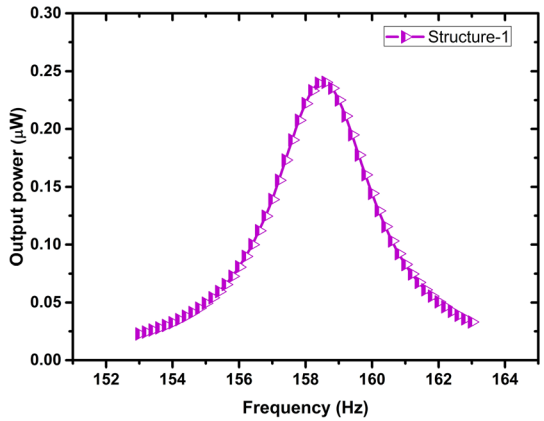

Fig. 9 Power Vs Frequency plot for structure-1

harvester with a rectangular beam and rectangular proof mass.

This continuous structure is useful as far as array-based energy harvesters are considered. Generally in array-based structures using rectangular beam and rectangular proof mass, the die area is not utilized efficiently due to the larger proof mass width. On the other hand, the proposed structure can be incorporated to design array-based energy harvesters by efficiently utilizing the die area.

3.4 Effect of the amount of proof mass coverage on the performance parameters

In this section, the effect of the amount of proof mass coverage on the output power and resonant frequency are analysed. The total length of the structure is kept constant at 10 mm. Then the proof mass length is varied in such a way that the ratio of proof mass length to overall length of the harvester changes from 10 % to 95 %. The obtained result is shown in Fig. 10.

From Fig. 10 it can be observed that the resonant frequency decreases initially, reaches a minimum value and

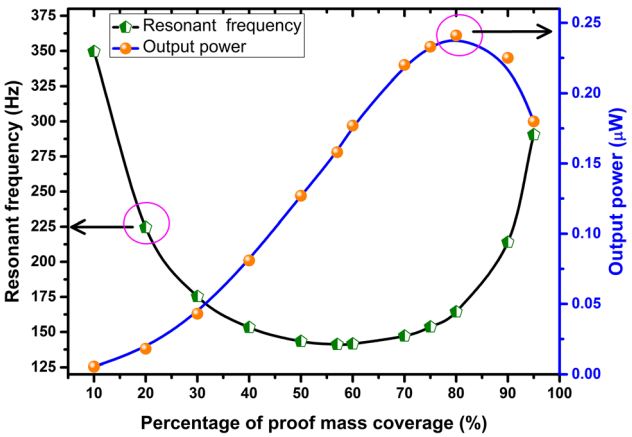

Fig. 10 Effect of proof mass coverage on the resonant frequency and output power

increases again as the proof mass coverage increases. The lowest resonant frequency is achieved when the proof mass coverage is 57 % of the overall length. Also, the output power is peaking when the proof mass coverage is almost 80 % of the overall length. Therefore, while designing an energy harvester there should be a trade-off between the lowest resonant frequency and peak output power. Thus the optimum amount of proof mass coverage can be selected as 70 % to 80 % so that power in μW levels can be attained at a relatively low resonant frequency (<200 Hz), which in turn can be used for powering WSNs used for condition monitoring such as tire pressure monitoring, speed/acceleration monitoring in the automobile industry and structural health monitoring of buildings and bridges.

4 Array of energy harvesters

In this section, an array design of energy harvester using the proposed trapezoidal beam with a triangular proof mass is presented. Also, a comparative study is carried out with an array design consisting of the conventional energy harvester with a rectangular beam and a rectangular proof mass. The simulated structures of the two types of array harvesters are shown in Fig. 11. Here the area of the total array is 1 cm × 1 cm.

From Fig. 11 it can be observed that the number of cantilevers that can be accommodated in the given area is more if triangular-shaped energy harvesters are used. Here the total number of cantilevers for the array of rectangular energy harvester is 16, whereas the number of the triangular cantilever is 27. The major objective of the array design is to enhance the total output power. The graph of Power Vs Frequency for the two types of array structures at the optimum load resistance is shown in Fig. 12.

From the above analysis, it is observed that the array using the proposed structure provides better output power at a lower resonant frequency. Next, the harvested power from the two types of array structures at various loads is analyzed. The load resistance is varied from 10 KΩ to 2 MΩ. Figure. 13 shows the power and voltage responses at different load resistance values for the two array energy harvesters.

The peak output power generated is 6.69 μW at a load resistance of 275 KΩ and 3.74 μW at a load resistance of 450 KΩ for the array of triangular harvester and array of rectangular harvester respectively. The corresponding output voltages are 1.36 V and 1.29 V respectively. Thus the proposed structure generates 1.79 times more power at a lower frequency than the conventional structure.

5 Electromechanical modeling

In this section, the effect of the shape of the proof mass on the resonant frequency and output power of the energy harvester is presented. The parameters which affect the resonant frequency are the mass and length of the energy harvester. Mathematical modeling was done for the resonant frequency of a rectangular beam with different shapes

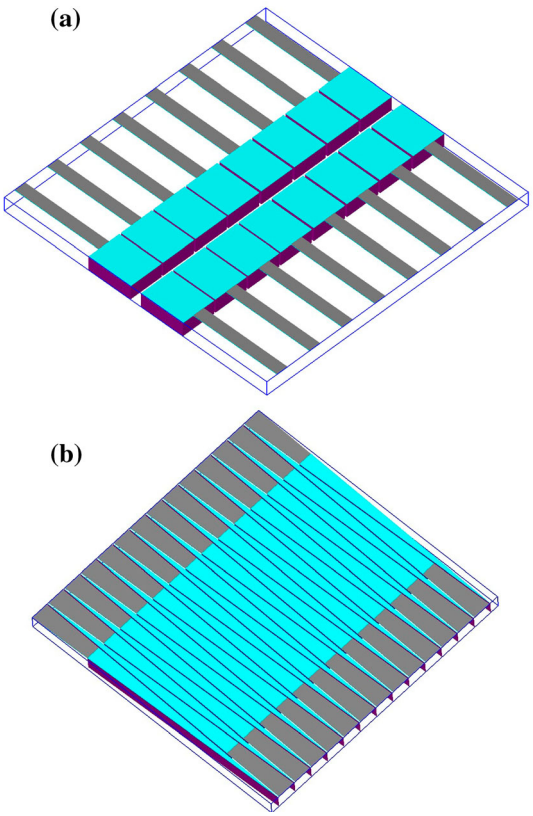

Fig. 11 Simulated structures of the array-based energy harvester (**a**) Rectangular (**b**) Triangular

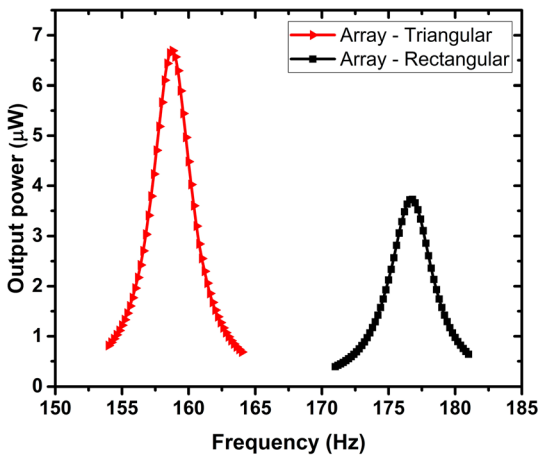

Fig. 12 Comparison of Output power Vs Frequency for array-based energy harvesters

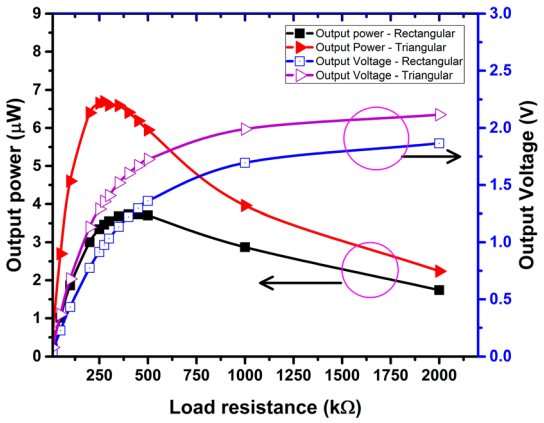

Fig. 13 Comparison of the output power and the output voltage for the array-based energy harvesters

of proof masses. Mainly three geometries of the proof mass have been analyzed namely Rectangular, Triangular, and Semi-circular. Here for analysing the effect of proof mass geometry on the resonant frequency first a rectangular beam is selected which carries a proof mass at its tip. The length and width of the beam are assumed to be constant for all the three proof mass geometries. Also, the thickness of each layer contributing to the mass is assumed to be constant. Then for a given mass, the only varying parameter is length/width of the proof mass. From the existing model given in Eq. (4) which is applicable for a rectangular beam with rectangular proof mass, the term equivalent length is the parameter to be modeled.

5.1 Energy harvester with a rectangular proof mass

Consider an energy harvester that consists of a rectangular beam of length l_b and a rectangular proof mass of length l_{pm} as shown in Fig. 14. Here the centroid of the rectangular proof mass (c) is located at a distance of $\frac{l_{pm}}{2}$ from the base of the rectangular proof mass.

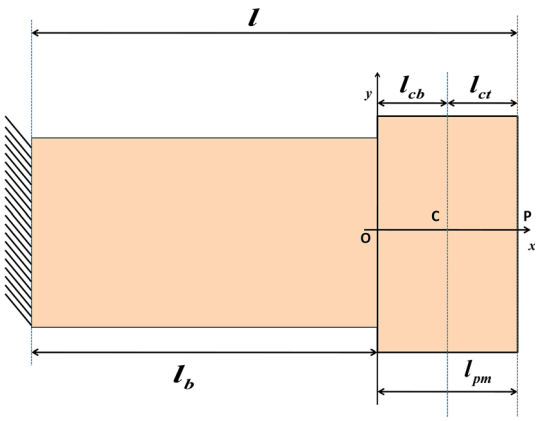

Fig. 14 Energy harvester with a rectangular proof mass

Thus the distance to centroid from the base of the rectangle in the x-direction is given by Eq. (8).

$$l_{cb} = \frac{l_{pm}}{2} \tag{8}$$

Therefore the distance to centroid from the tip of the energy harvester is given by Eq. (9).

$$l_{ct} = \frac{l_{pm}}{2} \tag{9}$$

Thus, for an energy harvester having a rectangular beam and rectangular proof mass equivalent length is given by Eq. (10).

$$L = l - \frac{l_{pm}}{2} \tag{10}$$

Where l is the total length of the energy harvester given by Eq. (11)

$$l = l_b + l_{pm} \tag{11}$$

Thus the resonant frequency of a rectangular beam with a rectangular proof mass can be written as Eq. (12)

$$f_r = \frac{1}{2\pi}\sqrt{\frac{3EI}{\left(m_{pm} + \frac{33}{140}m_s\right)\left(l - \frac{l_{pm}}{2}\right)^3}} \tag{12}$$

Therefore the maximum output power that can be generated by an energy harvester with rectangular proof mass can be written as

$$P_{rmax} = \frac{m_e A^2}{16\zeta\sqrt{\frac{3EI}{\left(m_{pm}+\frac{33}{140}m_s\right)\left(l-\frac{l_{pm}}{2}\right)^3}}} \tag{13}$$

5.2 Energy harvester with a triangular proof mass

Consider an energy harvester that consists of a rectangular beam and a triangular proof mass as shown in Fig. 15. Here the centroid of the triangular proof mass is located at a distance of $\frac{l_{pm}}{3}$ rather than $\frac{l_{pm}}{2}$ from the base of the triangular proof mass.

Thus the distance to centroid from the base of triangle in the x-direction is given by Eq. (14).

$$l_{cb} = \frac{l_{pm}}{3} \tag{14}$$

Therefore the distance to centroid from the tip of the energy harvester is given by Eq. (15).

$$l_{ct} = \frac{2l_{pm}}{3} \tag{15}$$

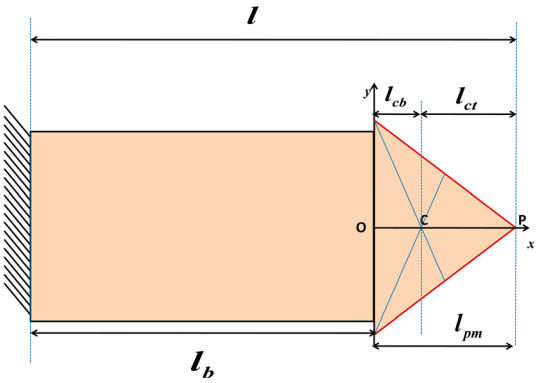

Fig. 15 Energy harvester with a triangular proof mass

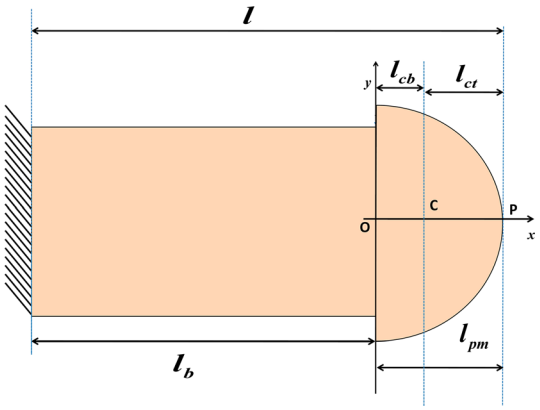

Fig. 16 Energy harvester with a semi-circular proof mass

From Eq. (10) it can be seen that the equivalent length is given as a difference of the total length of the harvester and distance to the centroid of the proof mass from the tip of the harvester.

Thus, for an energy harvester with a rectangular beam and a triangular proof mass, the equivalent length can be expressed by Eq. (16)

$$L = l - \frac{2l_{pm}}{3} \tag{16}$$

Thus the resonant frequency of a rectangular beam with a triangular proof mass can be written as Eq. (17)

$$f_t = \frac{1}{2\pi}\sqrt{\frac{3EI}{\left(m_{pm} + \frac{33}{140}m_s\right)\left(l - \frac{2l_{pm}}{3}\right)^3}} \tag{17}$$

Therefore the maximum output power that can be generated by an energy harvester with a triangular proof mass can be written as

$$P_{tmax} = \frac{m_e A^2}{16\zeta\sqrt{\frac{3EI}{\left(m_{pm}+\frac{33}{140}m_s\right)\left(l-\frac{2l_{pm}}{3}\right)^3}}} \tag{18}$$

5.3 Energy harvester with a semi-circular proof mass

Consider an energy harvester that consists of a rectangular beam and a semi-circular proof mass as shown in Fig. 16.

Here the centroid of the semi-circular proof mass is located at a distance of $\frac{4l_{pm}}{3\pi}$ rather than $\frac{l_{pm}}{2}$ from the base of the semicircular proof mass. Therefore the distance to centroid from the base of the semi-circular proof mass in the x-direction is given by Eq. (19)

$$l_{cb} = \frac{4r}{3\pi} = \frac{4l_{pm}}{3\pi} \tag{19}$$

Where 'r' is the radius of the semi-circle, which is equal to the length of the proof mass l_{pm}. Therefore the distance to centroid from the tip of the energy harvester is given by Eq. (20)

$$l_{ct} = \frac{5.425l_{pm}}{3\pi} \tag{20}$$

Therefore the effective length of the energy harvester with a semi-circular proof mass becomes

$$L = l - \frac{5.425l_{pm}}{3\pi} \tag{21}$$

Thus the resonant frequency of a rectangular beam with a semi-circular proof mass can be written as Eq. (22)

$$f_s = \frac{1}{2\pi}\sqrt{\frac{3EI}{\left(m_{pm} + \frac{33}{140}m_s\right)\left(l - \frac{5.425l_{pm}}{3\pi}\right)^3}} \tag{22}$$

Therefore the maximum output power that can be generated by an energy harvester with semi-circular proof mass can be written as

$$P_{smax} = \frac{m_e A^2}{16\zeta\sqrt{\frac{3EI}{\left(m_{pm}+\frac{33}{140}m_s\right)\left(l-\frac{5.425l_{pm}}{3\pi}\right)^3}}} \tag{23}$$

Thus from Eqs. (12), (17) and (22), it is evident that the resonant frequency of an energy harvester is effected by the geometry of the proof mass which in turn affects the output power.

5.4 Validation of the model

The effect of proof mass geometry on the resonant frequency given by Eqs. (12) (17) and (22), are validated using MATLAB. Analytical and simulation results are found to be in close proximity as shown in Fig. 17.

Figure 18 shows a comparison of output power for the three proof mass geometries. From Fig. 18 it can be observed that the energy harvester with triangular proof mass provides more power than rectangular and semi-

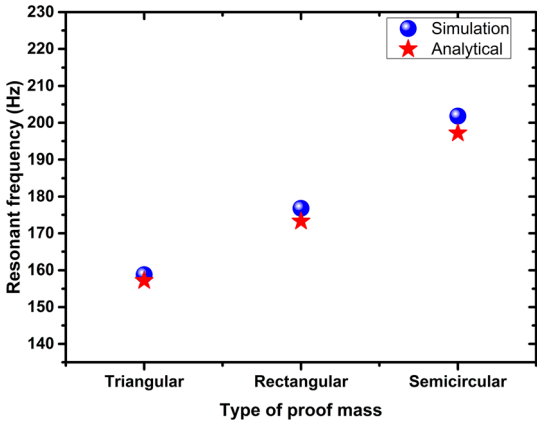

Fig. 17 Resonant frequency Vs Proof mass geometry

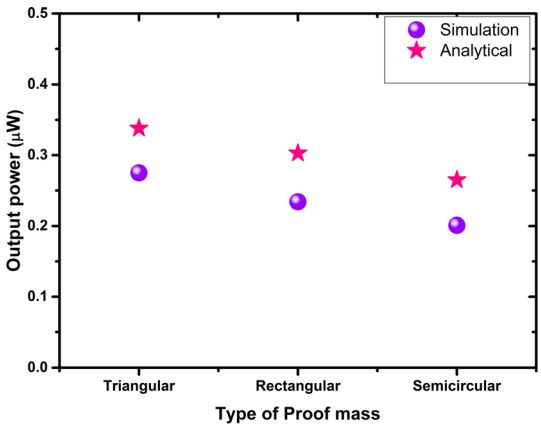

Fig. 18 Output power Vs Proof mass geometry

circular proof mass. The simulation results have slightly deviated from the analytical values. The probable reason can be the slight mismatch in mechanical and electrical damping ratios.

6 Conclusions

A new design of the Piezoelectric vibration energy harvester is proposed to obtain higher output power at a lower resonant frequency. The proposed structure consists of a trapezoidal beam with a triangular proof mass. The effect of the ratio of proof mass length to the total length of the harvester, on resonant frequency and output power, is analysed in detail. It is found that for a given length, the resonant frequency will be the least when the proof mass coverage is 57 % of the overall length. Also, the output power is peaking when the proof mass coverage is almost 80 % of the overall length. Therefore, while designing an energy harvester there should be a trade-off between the lowest resonant frequency and peak output power. The proposed structure generated output power of 0.24 μW at a resonant frequency of 158.8 Hz when excited by an input acceleration of 0.5 g. Then an array of trapezoidal cantilevers with the triangular proof mass is simulated and compared with the array of energy harvester consisting of rectangular cantilevers with the rectangular proof mass for a given area. It is found that the number of cantilevers that can be accommodated in the given area is more if the proposed trapezoidal cantilever with triangular proof mass is used when compared to a conventional rectangular beam with rectangular proof mass. The array using the proposed structure was able to generate 6.69 μW at 158.8 Hz, whereas the rectangular array was able to generate only 3.73 μW at 176.4 Hz. Thus the array using the proposed structure provides 1.79 times higher power at a lower resonant frequency than the conventional array. Electromechanical modeling of an energy harvester with a rectangular beam and different proof mass shapes is carried out. The simulation results are validated using MATLAB. Therefore the new design provides an enhancement in the performance of piezoelectric energy harvesters, in terms of resonant frequency and power density, which is highly desirable for energy harvesters to be used as a powering source for WSNs.

References

Alameh A, Gratuze M, Elsayed M, Nabki F (2018) Effects of proof mass geometry on piezoelectric vibration energy harvesters. Sensors 18(5):1584

Anton SR, Sodano HA (2007) A review of power harvesting using piezoelectric materials (2003–2006). Smart Materials Struct 16(3):R1

Bai P, Zhu G, Lin ZH, Jing Q, Chen J, Zhang G, Ma J, Wang ZL (2013) Integrated multilayered triboelectric nanogenerator for harvesting biomechanical energy from human motions. ACS Nano 7(4):3713

Beeby SP, Tudor MJ, White N (2006) Energy harvesting vibration sources for microsystems applications. Measure Sci Technol 17(12):R175

Chandrasekhar A, Alluri NR, Sudhakaran M, Mok YS, Kim SJ (2017) A smart mobile pouch as a biomechanical energy harvester towards self-powered smart wireless power transfer applications. Nanoscale 9(28):9818

Chandrasekhar A, Alluri NR, Vivekananthan V, Purusothaman Y, Kim SJ (2017) A sustainable freestanding biomechanical energy harvesting smart backpack as a portable-wearable power source. J Materials Chem C 5(6):1488

Chandrasekhar A, Vivekananthan V, Khandelwal G, Kim SJ (2019) Sustainable human-machine interactive triboelectric nanogenerator toward a smart computer mouse. ACS Sustain Chem Eng 7(7):7177

Chandrasekhar A, Vivekananthan V, Kim SJ (2020) A fully packed spheroidal hybrid generator for water wave energy harvesting and self-powered position tracking. Nano Energy 69:104439

Eom CB, Trolier-McKinstry S (2012) Thin-film piezoelectric MEMS. Mrs Bull 37(11):1007

Fei C, Liu X, Zhu B, Li D, Yang X, Yang Y, Zhou Q (2018) AlN piezoelectric thin films for energy harvesting and acoustic devices. Nano Energy 51:146

Gilbert JM, Balouchi F (2008) Comparison of energy harvesting systems for wireless sensor networks. Int J Automation Comput 5(4):334

Jackson N, o'Keeffe R, Waldron F, O'Neill M, Mathewson A, (2014) Evaluation of low-acceleration MEMS piezoelectric energy harvesting devices. Microsyst Technol 20(4–5):671

Jia Y, Seshia AA (2016) Five topologies of cantilever-based MEMS piezoelectric vibration energy harvesters: a numerical and experimental comparison. Microsyst Technol 22(12):2841

Kim SB, Park H, Kim SH, Wikle HC, Park JH, Kim DJ (2012) Comparison of MEMS PZT cantilevers based on d_31 and d_33 modes for vibration energy harvesting. J Microelectromech Syst 22(1):26

Nisanth A, Suja K, Seena V (2018) In: 2018 IEEE SENSORS (IEEE), pp. 1–4

Priya S, Inman DJ (2009) Energy harvesting technologies, vol 21. Springer, Berlin

Ramsay MJ, Clark WW (2001) In: Smart structures and materials 2001: industrial and commercial applications of smart structures technologies, vol 4332 (International Society for Optics and Photonics), vol. 4332, pp. 429–439

Roundy S, Wright PK (2004) A piezoelectric vibration based generator for wireless electronics. Smart Materials Struct 13(5):1131

Roundy S, Wright PK, Rabaey J (2003) A study of low level vibrations as a power source for wireless sensor nodes. Comput Commun 26(11):1131

Saadon S, Sidek O (2011) A review of vibration-based MEMS piezoelectric energy harvesters. Energy Conversion Manag 52(1):500

Saxena S, Sharma R (2014) Effect of shape of seismic mass on potential generated by MEMS-based cantilever-type piezoelectric energy harvester. J Micro/Nanolithography MEMS MOEMS 13(3):033012

Seah WK, Eu ZA, Tan HP (2009) In: 2009 1st international conference on wireless communication, vehicular technology, information theory and aerospace & electronic systems technology (Ieee), pp 1–5

Shen D, Park JH, Noh JH, Choe SY, Kim SH, Wikle HC III, Kim DJ (2009) Micromachined PZT cantilever based on SOI structure for low frequency vibration energy harvesting. Sens Actuat A 154(1):103

Sordo G, Serra E, Schmid U (1811) Iannacci J (2016) Optimization method for designing multimodal piezoelectric MEMS energy harvesters. Microsyst Technol 22(7):

Sukumaran C, Vivekananthan V, Mohan V, Alex ZC, Chandrasekhar A, Kim SJ (2020) Triboelectric nanogenerators from reused plastic: an approach for vehicle security alarming and tire motion monitoring in rover. Appl Materials Today 19:100625

Todaro MT, Guido F, Mastronardi V, Desmaele D, Epifani G, Algieri L, De Vittorio M (2017) Piezoelectric MEMS vibrational energy harvesters: advances and outlook. Microelectron Eng 183:23

Toprak A (1989) Tigli O (2015) MEMS scale PVDF-TrFE-based piezoelectric energy harvesters. J Microelectromech Syst 24(6):

Wei C, Jing X (2017) A comprehensive review on vibration energy harvesting: Modelling and realization. Renew Sustain Energy Rev 74:1

Williams C, Yates RB (1996) Analysis of a micro-electric generator for microsystems. Sens Actuat A 52(1–3):8

Yu H, Zhou J, Deng L, Wen Z (2014) A vibration-based MEMS piezoelectric energy harvester and power conditioning circuit. Sensors 14(2):3323

Zhang G, Gao S, Liu H, Niu S (2017) A low frequency piezoelectric energy harvester with trapezoidal cantilever beam: theory and experiment. Microsystem Technologies 23(8):3457